Available online at www.sciencedirect.com
SCIENCE DIRECT®
Journal of Sound and Vibration 281 (2005) 627–645
JOURNAL OF SOUND AND VIBRATION
www.elsevier.com/locate/jsvi

Free vibration analysis of conical shells via the element-free kp-Ritz method

K.M. Liew[a,b,*], T.Y. Ng[a,b], X. Zhao[a]

[a]*Nanyang Centre for Supercomputing and Visualisation, Nanyang Technological University, Nanyang Avenue, 639798 Singapore*
[b]*School of Mechanical and Production Engineering, Nanyang Technological University, Nanyang Avenue, 639798 Singapore*

Received 20 May 2003; received in revised form 2 January 2004; accepted 28 January 2004
Available online 18 September 2004

Abstract

In this paper, we consider the free vibration analysis of thin conical shells under different boundary conditions. The analysis is carried out using the element-free kp-Ritz method. The present study is based on the classical thin-shell theory. The kernel particle (kp) functions are employed in hybridized form with harmonic functions to approximate the two-dimensional displacement field. In order to examine the numerical stability of the present approach, convergence studies are performed based on the influences of the support size and the number of nodes. To verify the accuracy of this method, comparisons of the present results are made with results available in the open literature. This study also examines in detail the effects of semi-vertex angles and boundary conditions on the frequency characteristics of the conical shells.

1. Introduction

Conical shells have found wide applications as components in practical engineering structures, and the vibration analysis of such components is important for the safety and stability of the

*Corresponding author. School of Mechanical & Production Engineering, Nanyang Centre for Supercomputing and Visualisation, Nanyang Technological University, Singapore 639798, Singapore. Tel.: +65-6790-4076; fax: +65-6793-6763.
E-mail address: mkmliew@ntu.edu.sg (K.M. Liew).

0022-460X/$ - see front matter
doi:10.1016/j.jsv.2004.01.005

structure. The equations of motion for conical shells were summarized by Leissa [1], according to the various thin shell theories. Based on these different shell theories, many researchers studied the vibration of various conical shell problems. Some notable works include those by Saunders et al. [2], Garnet and Kemper [3] and Siu and Bert [4]. In these works, the Ritz method was used to obtain the natural frequencies. Irie et al. [5,6] studied the free vibration of conical shells with variable thickness using the transfer matrix method. A spline finite strip method was employed by Cheung et al. [7] to study the free vibration of singly curved shells. The vibration analysis of isotropic and laminated composite truncated conical shells, with consideration for transverse shear deformation, was carried out by Kayran and Vinson [8] using a combination of modal iteration and transfer matrix approaches. Sivadas and Ganesan [9,10] investigated the effects of thickness variation on natural frequencies of laminated conical shells by a semi-analytical finite element method. Tong [11,12] proposed the power series expansion approach to study the free vibration of orthotropic and composite laminated conical shells. Shu [13] employed the differential quadrature method to study the vibration of conical shells. Lam and Li [14] used the Galerkin method to examine the influence of boundary conditions on the frequency characteristics of a rotating truncated circular conical shell. A global Ritz formulation was presented by Lim and Liew [15] to study the vibratory behavior of shallow conical shells. The effects of initial twist and thickness variation on the vibration behaviour of the shallow conical shells were investigated [16]. Liew et al. [17] and Lim and Liew [18] also studied the vibration of cantilevered conical shells. Some of their works also included the vibration of conical shells with shear flexibility [19], and vibration of conical shell panels with three-dimensional flexibility [20].

The Ritz method [21], a generalization of the Rayleigh method [22], is a proven approximate technique extensively used in computational mechanics. It is a method that is highly dependent upon its trial functions. Examples of these trial functions used in 2-D analyses included the products of eigenfunctions of vibrating beams (Refs. [23–26]), orthogonal characteristic beam polynomials (Refs. [27,28]), and 2-D orthogonal plate functions (Refs. [29,30]) and 2-D basic polynomials used in the p-version Ritz method (Ref. [31]). In the present work, the free vibration analysis of conical shells is studied using the mesh-free kp-Ritz method [32]. This method is developed based on the kernel particle concept; the hybrid displacement field is approximated by the product of kernel particle (kp) functions in the longitudinal direction, and harmonic functions in the circumferential direction. By combining the kernel particle concept with the Ritz procedure, eigenequations for the free vibration of conical shells are derived. Discussion of our results, focusing on the effects of the semi-vertex angles and boundary conditions on the frequency characteristics of the conical shells, is presented.

2. kp-Ritz formulation

2.1. Energy formulation

Fig. 1 (a) shows the geometry of a thin truncated circular conical shell with semi-vertex cone angle α, length L and thickness h. R_1 and R_2 are the radii at the two ends. A coordinate system (x, θ, z) is fixed on the mid-surface of the shell. The displacements of the shell in the x, θ and z directions are denoted by u, v, and w, respectively. The cone radius at any point along its length is

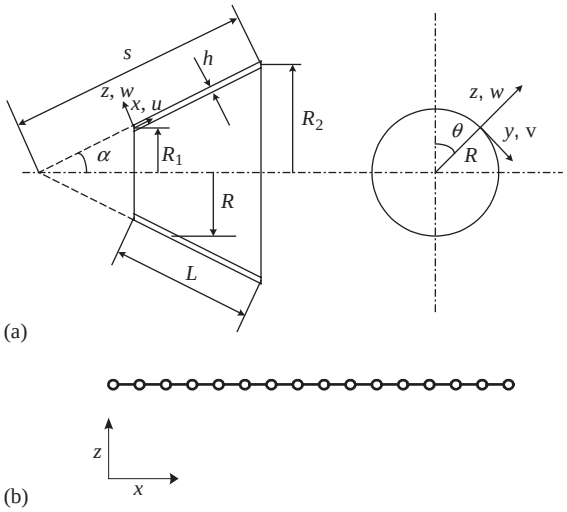

Fig. 1. (a) Geometry of the circular conical shell, (b) nodal arrangement in the longitudinal direction.

given by

$$R(x) = R_1 + x \sin \alpha. \tag{1}$$

The kinetic energy of the conical shell is expressed as

$$T = \tfrac{1}{2}\rho h \int_0^L \int_0^{2\pi} (\dot{u}^2 + \dot{v}^2 + \dot{w}^2) R(x)\, \mathrm{d}\theta\, \mathrm{d}x \tag{2}$$

and the strain energy is given by

$$U_\varepsilon = \frac{1}{2} \int_0^L \int_0^{2\pi} \boldsymbol{\varepsilon}^{\mathrm{T}} \mathbf{S} \boldsymbol{\varepsilon} R(x) \mathrm{d}\theta \mathrm{d}x, \tag{3}$$

where $\boldsymbol{\varepsilon}^{\mathrm{T}}$ and $\mathbf{S}$ are the strain vector and stiffness matrix, respectively, and $\boldsymbol{\varepsilon}^{\mathrm{T}}$ is defined as

$$\boldsymbol{\varepsilon}^{\mathrm{T}} = \{e_1 \;\; e_2 \;\; \gamma \;\; \kappa_1 \;\; \kappa_2 \;\; 2\tau\}. \tag{4}$$

The mid-surface strains e_1, e_2 and γ and the mid-surface curvatures κ_1, κ_2 and τ are defined according to Love's shell theory as follows:

$$e_1 = \frac{\partial u}{\partial x}, \tag{5}$$

$$e_2 = \frac{1}{R(x)} \frac{\partial v}{\partial \theta} + \frac{u \sin \alpha}{R(x)} + \frac{w \cos \alpha}{R(x)}, \tag{6}$$

$$\gamma = \frac{\partial v}{\partial x} + \frac{1}{R(x)} \frac{\partial u}{\partial \theta} - \frac{v \sin \alpha}{R(x)}, \tag{7}$$

$$\kappa_1 = -\frac{\partial^2 w}{\partial x^2}, \tag{8}$$

$$\kappa_2 = -\frac{1}{R^2(x)}\frac{\partial^2 w}{\partial\theta^2} + \frac{\cos\alpha}{R^2(x)}\frac{\partial v}{\partial\theta} - \frac{\sin\alpha}{R(x)}\frac{\partial w}{\partial x}, \tag{9}$$

$$\tau = -\frac{1}{R^2(x)}\frac{\partial^2 w}{\partial x\,\partial\theta} + \frac{\cos\alpha}{R(x)}\frac{\partial v}{\partial x} + \frac{\sin\alpha}{R^2(x)}\frac{\partial w}{\partial\theta} - \frac{v\sin\alpha\cos\alpha}{R^2(x)} \tag{10}$$

while the stiffness matrix $\mathbf{S}$ is given by

$$\mathbf{S} = \begin{bmatrix} A_{11} & A_{12} & A_{16} & B_{11} & B_{12} & B_{16} \\ A_{12} & A_{22} & A_{26} & B_{12} & B_{22} & B_{26} \\ A_{16} & A_{26} & A_{66} & B_{16} & B_{26} & B_{66} \\ B_{11} & B_{12} & B_{16} & D_{11} & D_{12} & D_{16} \\ B_{12} & B_{22} & B_{26} & D_{12} & D_{22} & D_{26} \\ B_{16} & B_{26} & B_{66} & D_{16} & D_{26} & D_{66} \end{bmatrix}. \tag{11}$$

The extensional stiffnesses A_{ij}, extensional–bending coupling stiffnesses B_{ij}, and bending stiffnesses D_{ij} are defined as

$$(A_{ij}, B_{ij}, D_{ij}) = \int_{-h/2}^{h/2} Q_{ij}(1, z, z^2)\,\mathrm{d}z \tag{12}$$

and $\mathbf{Q}$ denotes the plane stress-reduced stiffness matrix

$$\mathbf{Q} = \begin{bmatrix} Q_{11} & Q_{12} & 0 \\ Q_{12} & Q_{22} & 0 \\ 0 & 0 & Q_{66} \end{bmatrix}. \tag{13}$$

For an isotropic case

$$Q_{11} = \frac{E}{1-v^2}, \quad Q_{12} = \frac{vE}{1-v^2},$$

$$Q_{22} = \frac{E}{1-v^2}, \quad Q_{66} = G, \tag{14}$$

where E is the elastic modulus, G the shear modulus, and v Poisson's ratio. Thus, the energy functional of the conical shell is described as

$$\Pi = T - U_\varepsilon. \tag{15}$$

2.2. Hybrid approximate displacement field

The approximation of the displacement functions are expressed in hybridized kernel particle (kp)-harmonic forms as

$$u(x,\theta)=\sum_{I=1}^{\mathrm{NP}}\psi_I(x)u_I\cos(n\theta+\omega t),$$

$$v(x,\theta)=\sum_{I=1}^{\mathrm{NP}}\psi_I(x)v_I\sin(n\theta+\omega t),$$

$$w(x,\theta)=\sum_{I=1}^{\mathrm{NP}}\psi_I(x)w_I\cos(n\theta+\omega t), \tag{16}$$

where NP is the total number of particles, $\psi_I(x)$ is the shape function along the axes of the displacements u, v and w. u_I, v_I and w_I are the unknown nodal values of u, v and w at a given point, and n is the circumferential half wavenumber. The nodal distribution in the longitudinal direction is shown in Fig. 1(b). In the present study, the nodes are considered to be uniformly distributed.

The kernel particle shape function is given by [33]

$$\psi_I(x)=C(x;x-x_I)\varphi_a(x-x_I), \tag{17}$$

where $C(x;x-x_I)$ is the correction function and $\varphi_a(x-x_I)$ is called the kernel function.

The correction function $C(x;x-x_I)$ is written as

$$C(x;x-x_I)=\mathbf{H}^{\mathrm{T}}(x-x_I)\mathbf{b}(x), \tag{18}$$

where

$$\mathbf{H}(x-x_I)=[1,x-x_I,(x-x_I)^2]^{\mathrm{T}}, \tag{19}$$

$$\mathbf{b}(x)=[b_0(x),b_1(x),b_2(x)]^{\mathrm{T}} \tag{20}$$

and $\mathbf{H}$ is a vector of quadratic basis, while $b_i(x)$ are the functions of x to be determined.

Thus, the shape function can be assembled as

$$\psi_I(x)=\mathbf{b}^{\mathrm{T}}(x)\mathbf{H}(x-x_I)\varphi_a(x-x_I) \tag{21}$$

and Eq. (21) can be rewritten as

$$\psi_I(x)=\mathbf{b}^{\mathrm{T}}(x)\mathbf{B}_I(x-x_I) \tag{22}$$

in which

$$\mathbf{B}_I(x-x_I)=\mathbf{H}(x-x_I)\varphi_a(x-x_I), \tag{23}$$

$$\mathbf{b}(x)=\mathbf{M}^{-1}(x)\mathbf{H}(0), \tag{24}$$

where the moment matrix $\mathbf{M}$ is a function of x, and $\mathbf{H}(0)$ is a constant vector.

The expressions of $\mathbf{M}$ and $\mathbf{H}(0)$ are given by

$$\mathbf{M}(x) = \sum_{I=1}^{\mathrm{NP}} \mathbf{H}(x - x_I)\mathbf{H}^{\mathrm{T}}(x - x)\varphi_a(x - x_I) \tag{25}$$

$$\mathbf{H}^{\mathrm{T}}(0) = [1, 0, 0] \tag{26}$$

and the shape function can therefore be expressed as

$$\psi_I(x) = \mathbf{H}^{\mathrm{T}}(0)\mathbf{M}^{-1}(x)\mathbf{H}(x - x_I)\varphi_a(x - x_I). \tag{27}$$

For thin shell problems, due to the governing differential equations being second orders, the first and second derivatives of the shape function need to be determined. The procedure to formulate the first derivative of the shape function is detailed as follows.

Firstly, Eq. (24) can be rewritten as

$$\mathbf{M}(x)\mathbf{b}(x) = \mathbf{H}(0), \tag{28}$$

where the vector $\mathbf{b}(x)$ can be determined using the LU decomposition of the matrix $\mathbf{M}(x)$, followed by the back substitution.

Taking the derivative of Eq. (28) leads to

$$\mathbf{M}_{,x}(x)\mathbf{b}(x) + \mathbf{M}(x)\mathbf{b}_{,x}(x) = \mathbf{H}_{,x}(0) \tag{29}$$

which can be rearranged as

$$\mathbf{M}(x)\mathbf{b}_{,x}(x) = \mathbf{H}_{,x}(0) - \mathbf{M}_{,x}(x)\mathbf{b}(x). \tag{30}$$

The first derivative of $\mathbf{b}(x)$ can be derived again using the LU decomposition procedure. The second derivative of $\mathbf{b}(x)$ can be determined by taking the derivative of Eq. (30) and using the same procedure.

The first derivative of the shape function is derived by taking the derivative of Eq. (27)

$$\psi_{I,x}(x) = \mathbf{b}_{,x}^{\mathrm{T}}(x)\mathbf{B}_I(x - x_I) + \mathbf{b}^{\mathrm{T}}(x)\mathbf{B}_{I,x}(x - x_I). \tag{31}$$

The second derivative of the shape function can be determined by taking derivative of Eq. (31) again

$$\psi_{I,xx}(x) = \mathbf{b}_{,xx}^{\mathrm{T}}(x)\mathbf{B}_I(x - x_I) + 2\mathbf{b}_{,x}^{\mathrm{T}}(x)\mathbf{B}_{I,x}(x - x_I) + \mathbf{b}^{\mathrm{T}}(x)\mathbf{B}_{I,xx}(x - x_I). \tag{32}$$

The kernel function is expressed as

$$\varphi_a = \frac{1}{d}\varphi\left(\frac{x - x_I}{d}\right), \tag{33}$$

where the dilation parameter d is the size of the support and $\varphi((x - x_I)/d)$ is the weight function.

In this study, the cubic spline function is chosen as the weight function

$$\varphi(z_I) = \begin{cases} \frac{2}{3} - 4z_I^2 + 4z_I^3 & \text{for } 0 \le |z_I| \le \frac{1}{2}, \\ \frac{4}{3} - 4z_I + 4z_I^2 - \frac{4}{3}z_I^3 & \text{for } \frac{1}{2} \le |z_I| \le 1, \\ 0 & \text{otherwise,} \end{cases} \tag{34a}$$

$$z_I = \frac{(x - x_I)}{d}. \tag{34b}$$

At a given node, the size of the domain of influence is calculated by

$$d_I = d_{\max} a_I, \tag{35}$$

where $d_{\max}$ is the scaling factor, which generally ranges from 2.0 to 4.0. The distance a_I is determined by searching for sufficient nodes to avoid singularity of the matrix $\mathbf{M}$. For a 1-D problem, each node should have at least two neighbors in its domain of influence.

To compute the derivatives of the shape function, it is necessary to determine the derivatives of the weight function. The first and second derivatives of weight function can be easily obtained using the chain rule of differentiation, i.e.

$$\frac{\mathrm{d}\varphi}{\mathrm{d}x} = \frac{\mathrm{d}\varphi}{\mathrm{d}z_I}\frac{\mathrm{d}z_I}{\mathrm{d}x} = \begin{cases} (-8z_I + 12z_I^2)\mathrm{sign}(x - x_I) & \text{for } 0 \le |z_I| \le \frac{1}{2}, \\ (-4 + 8z_I - 4z_I^2)\mathrm{sign}(x - x_I) & \text{for } \frac{1}{2} \le |z_I| \le 1, \\ 0 & \text{otherwise,} \end{cases} \tag{36a}$$

$$\frac{\mathrm{d}^2\varphi}{\mathrm{d}x^2} = \frac{\mathrm{d}^2\varphi}{\mathrm{d}z_I^2}\left(\frac{\mathrm{d}z_I}{\mathrm{d}x}\right)^2 = \begin{cases} (-8z_I + 24z_I) & \text{for } 0 \le |z_I| \le \frac{1}{2}, \\ (8 - 8z_I) & \text{for } \frac{1}{2} \le |z_I| \le 1, \\ 0 & \text{otherwise.} \end{cases} \tag{36b}$$

It is noted that the first and second derivatives of the weight function are continuous over the domain.

2.3. Enforcement of boundary conditions—a penalty approach

The boundary equations cannot be imposed directly due to the lack of delta properties in the shape function. In this study, the penalty method (see Ref. [34]), is employed for implementing the essential boundary conditions.

2.3.1. Simply supported boundary conditions

For a domain bounded by l_u, the essential boundary condition is given by

$$\mathbf{u} = \bar{\mathbf{u}} \quad \text{on } l_u, \tag{37}$$

in which $\bar{\mathbf{u}}$ is the prescribed displacement on the boundary l_u. Then, the variational form is expressed by

$$\Pi_{\bar{u}} = \frac{\bar{\alpha}}{2}\int_{l_u} (\mathbf{u} - \bar{\mathbf{u}})^{\mathrm{T}}(\mathbf{u} - \bar{\mathbf{u}})\,\mathrm{d}l, \tag{38}$$

where $\bar{\alpha}$ is a penalty parameter taken as $10^3 E$, and E being the Young's modulus of the material.

2.3.2. Clamped boundary conditions

For a domain bounded by l_u, besides the boundary condition described by Eq. (37), the rotation boundary condition is given by

$$\boldsymbol{\beta} = \bar{\boldsymbol{\beta}} \text{ on } l_u, \tag{39}$$

where

$$\boldsymbol{\beta} = \frac{\mathrm{d}\mathbf{u}}{\mathrm{d}\mathbf{x}} \tag{40}$$

and $\bar{\boldsymbol{\beta}}$ is the prescribed rotation on the boundary. The variational form due to the rotation is expressed by

$$\Pi_{\bar{\beta}} = \frac{\bar{\alpha}}{2}\int_{l_u} (\boldsymbol{\beta} - \bar{\boldsymbol{\beta}})^{\mathrm{T}}(\boldsymbol{\beta} - \bar{\boldsymbol{\beta}})\mathrm{d}l. \tag{41}$$

Therefore, the variational form due to the clamped boundary conditions can be expressed as

$$\Pi_B = \Pi_{\bar{u}} + \Pi_{\bar{\beta}}. \tag{42}$$

With the energy functional of Eq. (15), the total energy functional $\tilde{\Pi}$ for the shell is expressed as

$$\tilde{\Pi} = \Pi + \Pi_B. \tag{43}$$

2.4. kp-Ritz minimization

Substituting the displacement functions, Eq. (16), into the total energy functional, Eq. (43), and according to the following Ritz procedure:

$$\frac{\partial\tilde{\Pi}}{\partial u_I} = 0, \quad \frac{\partial\tilde{\Pi}}{\partial v_I} = 0, \quad \frac{\partial\tilde{\Pi}}{\partial w_I} = 0, \quad I = 1, 2, \ldots \text{NP} \tag{44}$$

and collation leads to the following matrix equation:

$$\left(\tilde{\mathbf{K}} - \omega^2\tilde{\mathbf{M}}\right)\hat{\mathbf{u}} = 0, \tag{45}$$

where

$$\tilde{\mathbf{K}} = \boldsymbol{\Lambda}^{-1}\mathbf{K}\boldsymbol{\Lambda}^{-\mathrm{T}}, \quad \tilde{\mathbf{M}} = \boldsymbol{\Lambda}^{-1}\mathbf{M}\boldsymbol{\Lambda}^{-\mathrm{T}} \tag{46}$$

$$\hat{\mathbf{u}} = [\hat{u}_1, \hat{v}_1, \hat{w}_1, \hat{u}_2, \hat{v}_2, \hat{w}_2, ..., \hat{u}_{\mathrm{NP}}, \hat{v}_{\mathrm{NP}}, \hat{w}_{\mathrm{NP}}] \tag{47}$$

in which

$$\boldsymbol{\Lambda}_{IJ} = \psi_I(x_J)\mathbf{I}, \ \mathbf{I} \text{ is identity matrix}, \tag{48}$$

$$\mathbf{K} = \mathbf{K}^{\varepsilon} + \mathbf{K}^{B_1} + \mathbf{K}^{B_2}, \tag{49}$$

$$\mathbf{K}_{IJ}^{\varepsilon} = \pi \int_0^L \mathbf{B}_I^{\varepsilon\mathrm{T}} \mathbf{S} \mathbf{B}_J^{\varepsilon} R(x)\,\mathrm{d}x, \tag{50}$$

$$\mathbf{K}_{IJ}^{\bar{B}_1} = \bar{\alpha}\pi \left[\int_{l_u} \mathbf{B}1_I^{B\mathrm{T}} \mathbf{B}1_J^{B} R(x)\,\mathrm{d}l + \int_{l_u} \mathbf{B}1_I^{B} \bar{\mathbf{u}} R(x)\,\mathrm{d}l \right], \tag{51}$$

$$\mathbf{K}_{IJ}^{B_2} = \bar{\alpha}\pi \left[\int_{l_u} \mathbf{B}2_I^{B\mathrm{T}} \mathbf{B}2_J^{B} R(x)\,\mathrm{d}l + \int_{l_u} \mathbf{B}2_I^{B} \bar{\beta} R(x)\,\mathrm{d}l \right], \tag{52}$$

$$\mathbf{M} = \rho h \pi \int_0^L \mathbf{M}_I^{\mathrm{T}} \mathbf{M}_J R(x)\,\mathrm{d}x \tag{53}$$

and

$$\mathbf{B}_I^{\varepsilon} = \begin{bmatrix} \dfrac{\partial \psi_I}{\partial x} & 0 & 0 \\ \dfrac{\sin\alpha}{R(x)}\psi_I & \dfrac{n}{R(x)}\psi_I & -\dfrac{\cos\alpha}{R(x)}\psi_I \\ -\dfrac{n}{R(x)}\psi_I & \dfrac{\partial \psi_I}{\partial x} - \dfrac{\sin\alpha}{R(x)}\psi_I & 0 \\ 0 & 0 & -\dfrac{\partial^2 \psi_I}{\partial x^2} \\ 0 & \dfrac{n\cos\alpha}{R^2(x)}\psi_I & \dfrac{n^2}{R^2(x)}\psi_I - \dfrac{\sin\alpha}{R(x)}\dfrac{\partial \psi_I}{\partial x} \\ 0 & \dfrac{2\cos\alpha}{R(x)}\dfrac{\partial \psi_I}{\partial x} - \dfrac{2\sin\alpha\cos\alpha}{R^2(x)}\psi_I & \dfrac{2n}{R(x)}\dfrac{\partial \psi_I}{\partial x} - \dfrac{2n\sin\alpha}{R^2(x)}\psi_I \end{bmatrix}, \tag{54}$$

$$\mathbf{B}1_I^B = \begin{bmatrix} \psi_I & 0 & 0 \\ 0 & \psi_I & 0 \\ 0 & 0 & \psi_I \end{bmatrix}, \quad \mathbf{B}2_I^B = \begin{bmatrix} \psi_{I,x} & 0 & 0 \\ 0 & \psi_{I,x} & 0 \\ 0 & 0 & \psi_{I,x} \end{bmatrix}, \tag{55}$$

$$\mathbf{M}_I^T = \begin{bmatrix} \psi_I & 0 & 0 \\ 0 & \psi_I & 0 \\ 0 & 0 & \psi_I \end{bmatrix}. \tag{56}$$

The integration of Eqs. (50)–(53) are computed using the Gauss integration, and the global mass and stiffness matrices are furnished by assembling the quadrature points that are gathered from the contributions at each node.

3. Example problems and numerical studies

In the present study, seven sets of boundary conditions are considered, namely, simply-supported–simply-supported (S_S–S_L), clamped–clamped (C_S–C_L), clamped–simply-supported (C_S–C_L), simply-supported–clamped (S_S–C_L), free–free (F_S–F_L), free–clamped (F_S–C_L), and

free–simply-supported (F_S–S_L). The subscript "s" denoted the edge with the smaller radius, while the subscript "L" denotes the edge with the larger radius. In the present numerical computation, Poisson's ratio is taken as $v = 0.3$, and the non-dimensional frequency parameter f is defined as

$$f = \omega R_2 \sqrt{\frac{\rho(1-v^2)}{E}}, \tag{57}$$

where ω is the natural frequency of the conical shell in radians per second.

3.1. Verification studies

To verify the present formulation and examine the accuracy of the present technique, convergence studies are conducted and comparisons with results available in open literature are made. The corresponding numerical results are tabulated in Tables 1–4.

Table 1 shows the convergence rate of the frequency parameter f for an isotropic conical shell of $\alpha = 60^\circ$, $L \sin \alpha / R_2 = 0.25$, $h/R_2 = 0.01$, with longitudinal wavenumber, $m = 1$. The number of nodes is varied from 20 to 50, and support size from 2.0 to 3.0. It is observed that the present method furnishes stable monotonic convergence characteristics. For a support size of 2.0, converged solutions can be achieved with 20 nodes. For support size of 2.5 and 3.0, converged results are obtained with 30 nodes. It is also observed that the results converge slightly faster when using a support size of 2.0 as compared to the other two larger support sizes. It is also noted that the convergence rate is independent of the circumferential wavenumber n. The present results are compared with solutions given by Irie [6], and excellent agreement is obtained for all modes.

To examine the effects of semi-vertex angle α on the convergence characteristics of the conical shells, convergence studies are performed for shells with $\alpha = 45^\circ$ and $\alpha = 60^\circ$. The results are respectively tabulated in Tables 2 and 3. Similar observations as those in Table 1 are evident. It can be observed from Tables 1–3 that the semi-vertex angle α does not affect convergence rates. Based on the above convergence studies, a support size of 2.0 is selected for all subsequent computations.

Table 1
Comparison of frequency parameter $f = \omega R_2 \sqrt{(1-v^2)\rho/E}$ for conical shell with S_S–S_L boundary conditions ($\alpha = 30^\circ$, $m = 1$, $v = 0.3$, $h/R_2 = 0.01$, $L \sin \alpha / R_2 = 0.25$)

n	Irie [6]	Present											
		$d_{max} = 2.0$				$d_{max} = 2.5$				$d_{max} = 3.0$			
		NP = 20	NP = 30	NP = 40	NP = 50	NP = 20	NP = 30	NP = 40	NP = 50	NP = 20	NP = 30	NP = 40	NP = 50
2	0.7910	0.7909	0.7909	0.7909	0.7909	0.7903	0.7903	0.7904	0.7905	0.7897	0.7901	0.7903	0.7904
3	0.7284	0.7281	0.7281	0.7281	0.7281	0.7268	0.7272	0.7275	0.7276	0.7262	0.7269	0.7272	0.7274
4	0.6352	0.6347	0.6347	0.6348	0.6348	0.6331	0.6337	0.6340	0.6341	0.6325	0.6332	0.6336	0.6339
5	0.5531	0.5522	0.5523	0.5523	0.5523	0.5506	0.5512	0.5515	0.5517	0.5500	0.5508	0.5512	0.5514
6	0.4949	0.4938	0.4938	0.4939	0.4939	0.4922	0.4928	0.4931	0.4932	0.4916	0.4924	0.4928	0.4930
7	0.4653	0.4639	0.4640	0.4640	0.4640	0.4625	0.4630	0.4633	0.4634	0.4620	0.4627	0.4630	0.4632
8	0.4654	0.4629	0.4629	0.4629	0.4629	0.4616	0.4621	0.4623	0.4625	0.4611	0.4618	0.4621	0.4623
9	0.4892	0.4875	0.4876	0.4876	0.4876	0.4863	0.4868	0.4870	0.4871	0.4860	0.4865	0.4868	0.4870

Table 2
Comparison of frequency parameter $f = \omega R_2\sqrt{(1-\upsilon^2)\rho/E}$ for conical shell with S_S–S_L boundary conditions ($\alpha = 45^\circ$, $m = 1$, $\upsilon = 0.3$, $h/R_2 = 0.01$, $L\sin\alpha/R_2 = 0.25$)

n	Irie [6]	Present											
		$d_{max} = 2.0$				$d_{max} = 2.5$				$d_{max} = 3.0$			
		NP = 20	NP = 30	NP = 40	NP = 50	NP = 20	NP = 30	NP = 40	NP = 50	NP = 20	NP = 30	NP = 40	NP = 50
2	0.6879	0.6877	0.6878	0.6878	0.6878	0.6869	0.6872	0.6874	0.6875	0.6866	0.6870	0.6872	0.6874
3	0.6973	0.6970	0.6971	0.6971	0.6971	0.6959	0.6963	0.6966	0.6967	0.6954	0.6960	0.6963	0.6965
4	0.6664	0.6659	0.6660	0.6660	0.6660	0.6644	0.6650	0.6653	0.6655	0.6638	0.6646	0.6650	0.6652
5	0.6304	0.6297	0.6298	0.6298	0.6298	0.6279	0.6286	0.6290	0.6292	0.6273	0.6282	0.6286	0.6289
6	0.6032	0.6023	0.6024	0.6024	0.6025	0.6004	0.6012	0.6015	0.6017	0.5997	0.6007	0.6012	0.6015
7	0.5918	0.5907	0.5908	0.5909	0.5909	0.5888	0.5895	0.5899	0.5901	0.5880	0.5890	0.5896	0.5899
8	0.5992	0.5980	0.5981	0.5981	0.5981	0.5960	0.5968	0.5972	0.5974	0.5953	0.5963	0.5968	0.5971
9	0.6257	0.6243	0.6244	0.6245	0.6245	0.6224	0.6232	0.6235	0.6238	0.6217	0.6227	0.6232	0.6235

Table 3
Comparison of frequency parameter $f = \omega R_2\sqrt{(1-\upsilon^2)\rho/E}$ for conical shell with S_S–S_L boundary conditions ($\alpha = 60^\circ$, $m = 1$, $\upsilon = 0.3$, $h/R_2 = 0.01$, $L\sin\alpha/R_2 = 0.25$)

n	Irie [6]	Present											
		$d_{max} = 2.0$				$d_{max} = 2.5$				$d_{max} = 3.0$			
		NP = 20	NP = 30	NP = 40	NP = 50	NP = 20	NP = 30	NP = 40	NP = 50	NP = 20	NP = 30	NP = 40	NP = 50
2	0.5722	0.5719	0.5720	0.5720	0.5721	0.5703	0.5710	0.5714	0.5715	0.5697	0.5706	0.5711	0.5713
3	0.6001	0.5998	0.5999	0.5999	0.6000	0.5980	0.5988	0.5992	0.5994	0.5974	0.5984	0.5989	0.5992
4	0.6054	0.6049	0.6050	0.6051	0.6051	0.6029	0.6038	0.6042	0.6045	0.6022	0.6033	0.6039	0.6042
5	0.6077	0.6071	0.6073	0.6073	0.6074	0.6049	0.6059	0.6063	0.6066	0.6041	0.6054	0.6060	0.6063
6	0.6159	0.6152	0.6153	0.6154	0.6154	0.6128	0.6138	0.6143	0.6146	0.6119	0.6133	0.6139	0.6143
7	0.6343	0.6335	0.6337	0.6337	0.6338	0.6310	0.6321	0.6326	0.6329	0.6301	0.6315	0.6322	0.6326
8	0.6650	0.6641	0.6643	0.6643	0.6644	0.6616	0.6627	0.6632	0.6635	0.6606	0.6621	0.6628	0.6631
9	0.7084	0.7075	0.7076	0.7077	0.7077	0.7049	0.7060	0.7065	0.7068	0.7040	0.7054	0.7061	0.7065

For a conical shell having $\alpha = 45^\circ$ and $L\sin\alpha/R_2 = 0.5$, Table 4 shows the comparison of present results with results reported by Irie [6] and Shu [13]. Four combinations of boundary conditions, S_S–S_L, S_S–C_L, C_L–S_S, and C_S–C_L, are considered here. The circumferential wavenumber, n, ranges from 0 to 9. In general, an excellent agreement is observed.

From the comparison studies carried out in Tables 1–4, it is concluded that the convergent results obtained by using a small support size and relatively less nodes. This conclusion indicates that the present method is numerically accurate and computationally efficient.

3.2. Numerical results

The variation of the frequency parameter f, see Eq. (57), of conical shells having S_S–S_L boundary conditions, with the semi-vertex angle α, are shown in Fig. 2. The longitudinal

Table 4
Comparison of frequency parameter $f = \omega R_2\sqrt{(1-\upsilon^2)\rho/E}$ for conical shell with different boundary conditions ($\alpha = 45^\circ$, m=1, $\upsilon = 0.3$, h/R_2=0.01, $L\sin\alpha/R_2 = 0.5$)

n	Boundary conditions											
	S_S–S_L			S_S–C_L			C_S–S_L			C_S–C_L		
	Shu [13]	Irie [6]	Present	Shu [13]	Irie [6]	Present	Shu [13]	Irie [6]	Present	Shu [13]	Irie [6]	Present
0	0.2233	0.2233	0.2234	0.8700	0.8698	0.8691	0.7151	0.7149	0.7148	0.8732	0.8731	0.8732
1	0.5463	0.5462	0.5462	0.8118	0.8117	0.8113	0.7098	0.7095	0.7095	0.8120	0.8120	0.8120
2	0.6310	0.6310	0.6309	0.6613	0.6614	0.6610	0.6475	0.6474	0.6473	0.6696	0.6696	0.6696
3	0.5062	0.5065	0.5061	0.5246	0.5249	0.5244	0.5201	0.5203	0.5199	0.5428	0.5430	0.5428
4	0.3942	0.3947	0.3941	0.4319	0.4324	0.4316	0.4161	0.4164	0.4158	0.4566	0.4570	0.4565
5	0.3340	0.3348	0.3337	0.3826	0.3834	0.3822	0.3592	0.3598	0.3589	0.4089	0.4095	0.4088
6	0.3239	0.3248	0.3235	0.3737	0.3747	0.3732	0.3450	0.3458	0.3446	0.3963	0.3970	0.3961
7	0.3514	0.3524	0.3510	0.3987	0.3997	0.3980	0.3648	0.3657	0.3644	0.4143	0.4151	0.4141
8	0.4023	0.4033	0.4019	0.4479	0.4489	0.4472	0.4093	0.4102	0.4088	0.4568	0.4577	0.4567
9	0.4676	0.4684	0.4671	0.5133	0.5142	0.5124	0.4706	0.4715	0.4701	0.5177	0.5186	0.5175

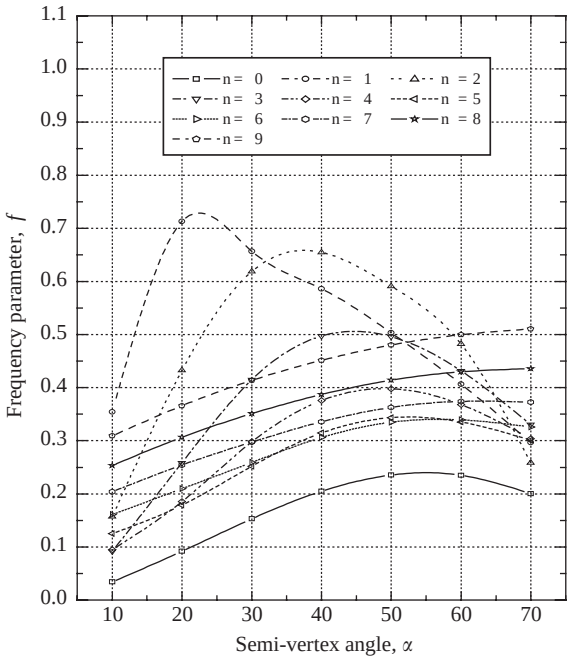

Fig. 2. Variation of frequency parameter f with semi-vertex angle α for a conical shell with S_S–S_L boundary conditions.

wavenumber is $m = 1$, while the circumferential wavenumber, n, ranges from 0 to 9, and α varies from 10° to 70°. A consistent trend is observed for the modes corresponding to $n = 0$ to 7, where the frequencies initially increase with increasing α and upon reaching a peak, the frequencies

decrease as α is further increased. However, the peak for each mode occurs at different α. For circumferential wavenumbers $n = 0$, 4 and 5, the peak frequencies occur at $\alpha = 50^\circ$. For circumferential wavenumber $n = 1$ the peak occurs at $\alpha = 20^\circ$. For the modes with $n = 2$ and 3, the peak frequencies occur at $\alpha = 40^\circ$, and correspondingly for $n = 6$ and 7, the peak frequencies occur at $\alpha = 60^\circ$. However, for circumferential wavenumbers with $n = 8$ and 9, the frequencies increase monotonously as angle α increases. From these results, it is concluded that the semi-vertex angle α has significant quantitative effects on the frequencies of the conical shell, and its effects on different modes are somewhat distinct. Fig. 3 correspondingly illustrates the variation of f with α, for conical shells of S_S–C_L boundary conditions. For modes with circumferential wavenumbers $n = 2$, 3, 4, 5, 6, 8 and 9, the same trends as those of the S_S–S_L case in Fig. 2 are observed. For the modes associated with $n = 0$ and 1, the peak frequencies occur at $\alpha = 20^\circ$ and $\alpha = 30^\circ$, respectively, while for the mode associated with $n = 7$, the frequencies increase in a monotonic manner as α increases.

In Fig. 4, the variation of f with α for conical shells having C_S–S_L boundary conditions is depicted. Similar trends as those in Fig. 2 for the S_S–S_L case are observed for modes associated with $n = 2-9$. For the two lower modes, i.e. $n = 0$ and 1, similar qualitative trends are observed except that the peaks now occur at $\alpha = 30^\circ$. For fully clamped C_S–C_L conical shells, the effects of α on the frequency characteristics are presented in Fig. 5. The same trends as those for the S_S–C_L case in Fig. 4 are observed. From Figs. 3 and 5, it is observed that the frequencies of the S_S–C_L conical shells have relatively less-significant differences with that of the C_S–C_L conical shells, whereas results for the S_S–C_L and C_S–S_L conical shells from the respective Figs. 3 and 4 display higher relative frequency differences.

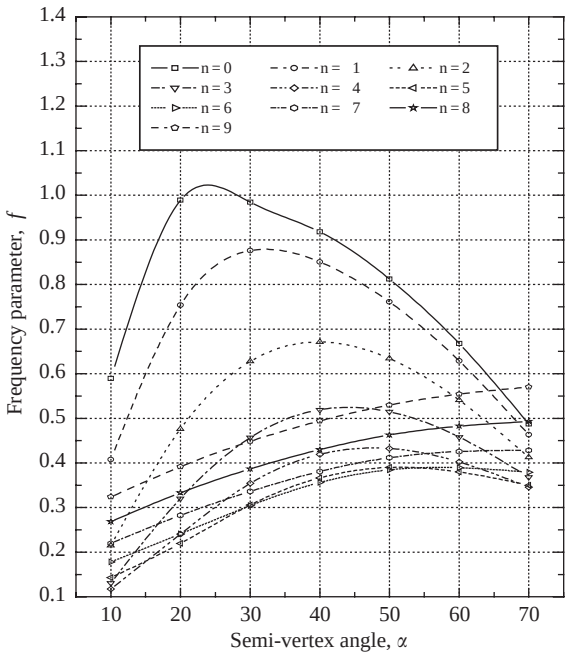

Fig. 3. Variation of frequency parameter f with semi-vertex angle α for a conical shell with S_S–C_L boundary conditions.

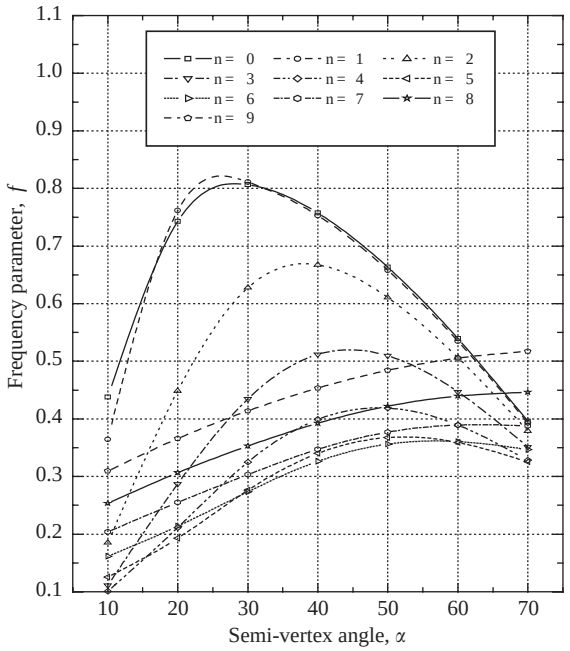

Fig. 4. Variation of frequency parameter f with semi-vertex angle α for a conical shell with C_S–S_L boundary conditions.

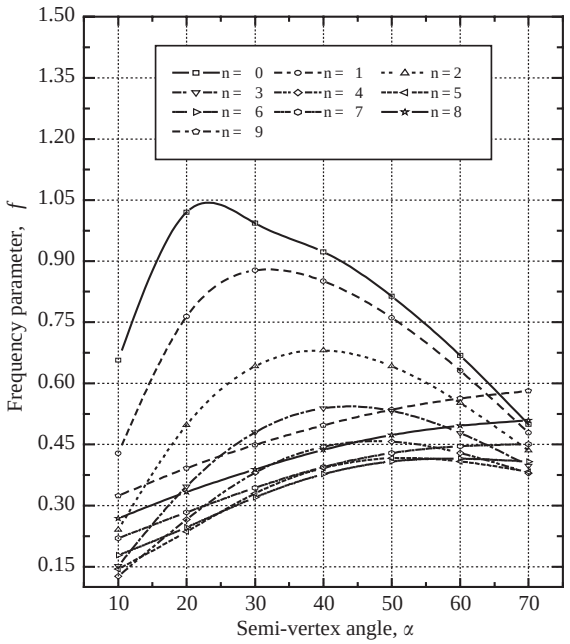

Fig. 5. Variation of frequency parameter f with semi-vertex angle α for a conical shell with C_S–C_L boundary conditions.

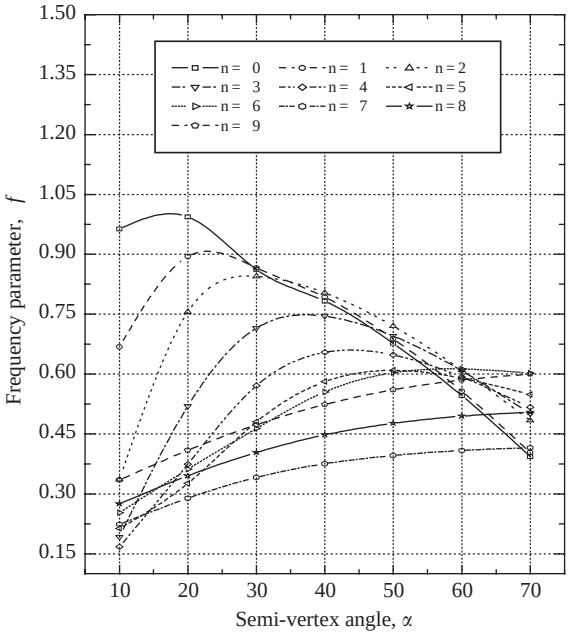

Fig. 6. Variation of frequency parameter f with semi-vertex angle α for a conical shell with F_S–F_L boundary conditions.

Fig. 6 shows the corresponding frequency results for completely free F_S–F_L conical shells. Very similar trends are observed in frequency variation for the corresponding modes as those in Fig. 5 for the C_S–C_L case. The only distinctions are that the frequency peaks for modes associated with $n = 1$ and 2 occur at $\alpha = 20^\circ$ and $\alpha = 30^\circ$, respectively. Fig. 7 presents the variation of f with α for conical shells having F_S–S_L boundary conditions. It is observed that the frequencies show similar trend as those of the F_S–F_L case in Fig. 6, for modes $n = 2$ to 9. For the two lower modes $n = 0$ and 1, maximum frequencies occur at $\alpha = 60^\circ$ instead of $\alpha = 20^\circ$. It is also noted that for these two modes $n = 0$ and 1, the frequencies for the F_S–S_L boundary condition case are significantly lower than that of the completely free F_S–F_L conical shells. Finally, Fig. 8 shows the corresponding frequency characteristics of conical shells having F_S–C_L boundary conditions. It is observed that the frequency variations are similar to those observed for the F_S–F_L case in Fig. 6, except that the maximum α for modes associated with $n = 2$, 4 and 5, are now respectively 30°, 50° and 55°.

Fig. 9 shows some mode shapes of conical shells with a semi-vertex angle $\alpha = 45^\circ$, having the S_S–S_L, S_S–C_L, C_S–S_L and C_S–C_L boundary conditions. The parameters used previously for generating results in Table 4 are again adopted here to obtain the present mode shapes. It is obvious that the effects of different boundary conditions on the mode shapes can be clearly observed.

3.3. Numerical observations

The applicability of the Ritz method for free vibration analysis of plates and shells has been well documented [1,31]. In this study, a major novel refinement in the manner in which the

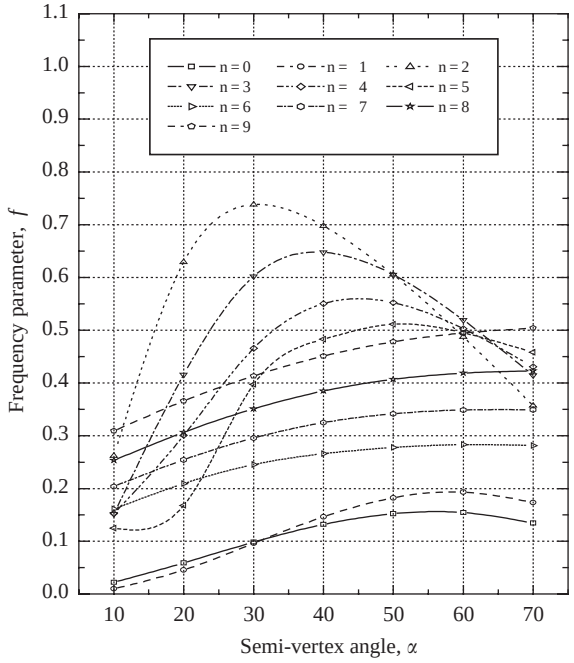

Fig. 7. Variation of frequency parameter f with semi-vertex angle α for a conical shell with F_S–S_L boundary conditions.

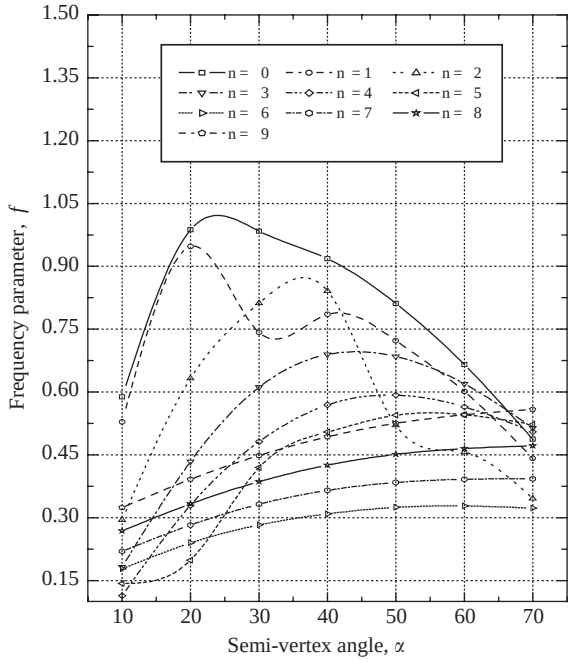

Fig. 8. Variation of frequency parameter f with semi-vertex angle α for a conical shell with F_S–C_L boundary conditions.

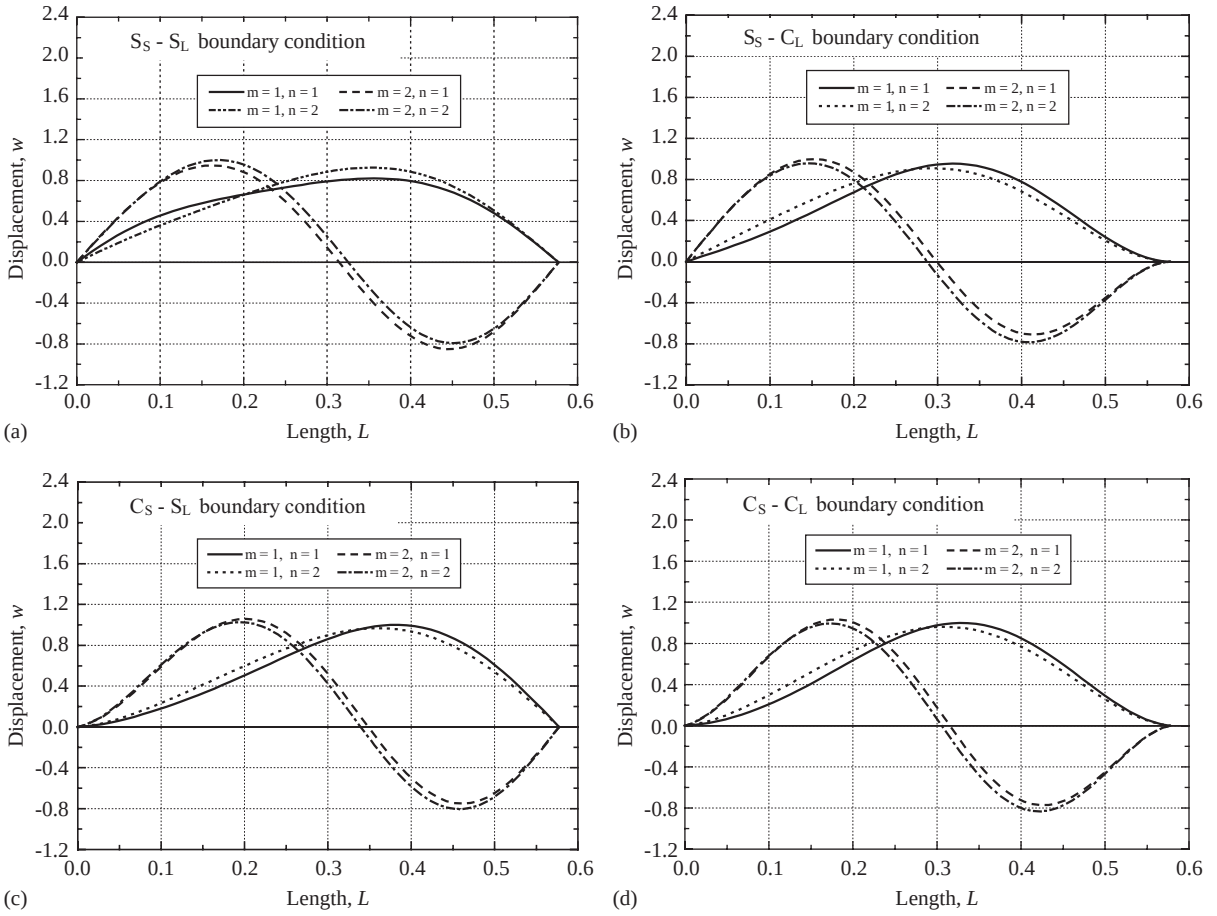

Fig. 9. Mode shapes for conical shell with different boundary conditions: (a) S_S–S_L; (b) S_S–C_L; (c) C_S–S_L; (d) C_S–C_L.

conventional Ritz method has been formulated. Furthermore, its feasibility to vibration study of conical shells was demonstrated. In the conventional Ritz method, the trial functions must satisfy at least the essential boundary conditions, and the difficulties of locating appropriate trial functions for certain boundary condition types have been well-known. The presently refinement and development of the kp-Ritz method have overcome this limitation, in which a common shape function type is used to generally describe the interior domain. The boundary conditions are separately dealt with subsequently through a penalty enforcement. This enhances the kp-Ritz method significantly, which is more robust than the conventional Ritz method.

Apart from being more robust, the kp-Ritz approach also leads to significant improvement in computational efficiency. For different boundary conditions when the conventional Ritz method is used, the eigenequations for each boundary condition will have to be reformulated. In the present kp-Ritz approach, however, only the variational line integral needs to be re-evaluated, leading to reduced computational efforts, and is comparatively simpler and easier to deal with.

4. Conclusions

The vibration analysis of conical shells has been successfully carried out via the mesh-free kp-Ritz method. The numerical stability of this method for conical shell analysis has been verified by extensive convergence studies. The computational accuracy has also been validated by comparisons with available published results. It is concluded that the present technique is accurate and efficient for the free vibration analysis of conical shells. Comprehensive parametric studies involving seven variations of boundary conditions was subsequently carried out, and it was found that the semi-vertex angle and boundary conditions significantly affect the frequency characteristics of the conical shells.

References

[1] A.W. Leissa, *Vibration of Shells*, Acoustic Society of America, New York, 1993.
[2] H. Saunders, E.J. Wisniewski, P.R. Paslay, Vibration of conical shells, *Journal of the Acoustical Society of America* 32 (1960) 765–772.
[3] H. Garnet, J. Kemper, Axisymmetric free vibration of conical shells, *Journal of Applied Mechanics* 31 (1964) 458–466.
[4] C.C. Siu, C.W. Bert, Free vibration analysis of sandwich conical shells with free edges, *Journal of the Acoustical Society of America* 47 (1970) 943–945.
[5] T. Irie, G. Yamada, Y. Kaneko, Free vibration of a conical shell with variable thickness, *Journal of Sound and Vibration* 82 (1982) 83–94.
[6] T. Irie, G. Yamada, Y. Kaneko, Natural frequencies of truncated conical shells, *Journal of Sound and Vibration* 92 (1984) 447–453.
[7] Y.K. Cheung, W.Y. Li, L.G. Tham, Free vibration analysis of singly curved shell by spline finite strip method, *Journal of Sound and Vibration* 128 (1989) 411–422.
[8] A. Kayran, J.R. Vison, Free vibration analysis of laminated composite truncated circular conical shells, *AIAA Journal* 28 (1990) 1259–1269.
[9] K.R. Sivadas, N. Ganesan, Vibration analysis of laminated conical shells with variable thickness, *Journal of Sound and Vibration* 148 (1991) 477–491.
[10] K.R. Sivadas, N. Ganesan, Vibration analysis of thick composite clamped conical shells of varying thickness, *Journal of Sound and Vibration* 152 (1992) 27–37.
[11] L.Y. Tong, Free vibration of orthotropic conical shells, *International Journal of Engineering Science* 31 (1993) 719–733.
[12] L.Y. Tong, Free vibration of composite laminated conical shells, *International Journal of Mechanical Sciences* 35 (1993) 47–61.
[13] C. Shu, An efficient approach for free vibration analysis of conical shells, *International Journal of Mechanical Sciences* 38 (1996) 935–949.
[14] K.Y. Lam, H. Li, Influence of boundary conditions on the frequency characteristics of a rotating truncated circular conical shell, *Journal of Sound and Vibration* 223 (1999) 171–195.
[15] C.W. Lim, K.M. Liew, Vibratory behaviour of shallow conical shells by a global Ritz formulation, *Engineering Structures* 17 (1) (1995) 63–70.
[16] K.M. Liew, M.K. Lim, C.W. Lim, D.B. Li, Y.R. Zhang, Effects of initial twist and thickness variation on the vibration behaviour of shallow conical shells, *Journal of Sound and Vibration* 180 (1995) 271–296.
[17] K.M. Liew, C.W. Lim, L.S. Ong, Vibration of pretwisted cantilever shallow conical shells, *International Journal of Solids and Structures* 31 (18) (1994) 2463–2476.
[18] C.W. Lim, K.M. Liew, S. Kitipornchai, Vibration of cantilevered laminated composite shallow conical shells, *International Journal of Solids and Structures* 35 (15) (1998) 1695–1707.

[19] C.W. Lim, K.M. Liew, Vibration of shallow conical shells with shear flexibility: a first-order theory, *International Journal of Solids and Structures* 33 (4) (1996) 451–468.
[20] K.M. Liew, Z.C. Feng, Vibration characteristics of conical shell panels with three-dimensional flexibility, *Journal of Applied Mechanics* 67 (2) (2000) 314–320.
[21] W. Ritz, Uber eine neue Methode zur Losung gewisser Variations probleme der mathematischen Physik, *Journal für Reine und Angewandte Mathematik* 135 (1909) 1–61.
[22] J.W. Rayleigh, *Theory of sound*, Vol. 1, Macmillian, New York, 1877 reprinted by Dover Publications, New York, 1945.
[23] S.M. Dickinson, E.K.K. Li, On the use of simply supported plate functions in the Rayleigh–Ritz method applied to the flexural vibration of rectangular plates, *Journal of Sound and Vibration* 80 (1982) 292–297.
[24] Y. Narita, A.W. Leissa, Buckling studies for simply supported symmetrically laminated rectangular plates, *International Journal of Mechanical Sciences* 32 (1990) 909–924.
[25] A.R. Kukreti, J. Farsa, C.W. Bert, Differential quadrature and Rayleigh–Ritz methods to determine the fundamental frequencies of simply supported rectangular plates with linearly varying thickness, *Journal of Sound and Vibration* 189 (1996) 103–122.
[26] Y.K. Cheung, D. Zhou, The free vibrations of tapered rectangular plates using a new set of beam functions with the Rayleigh–Ritz method, *Journal of Sound and Vibration* 223 (1999) 703–722.
[27] R.B. Bhat, Natural frequencies of rectangular plates using characteristic orthogonal polynomials in the Rayleigh–Ritz method, *Journal of Sound and Vibration* 102 (1985) 493–499.
[28] S.M. Dickinson, A.D. Blasio, On the use of orthogonal polynomials in the Rayleigh–Ritz method for the study of flexural vibration and buckling of isotropic and orthotropic rectangular plates, *Journal of Sound and Vibration* 108 (1986) 51–62.
[29] K.M. Liew, K.Y. Lam, S.T. Chow, Free vibration analysis of rectangular plates using orthogonal plate functions, *Computers and Structures* 34 (1990) 79–85.
[30] K.M. Liew, K.Y. Lam, Application of two-dimensional orthogonal plate function to flexural vibration of skew plates, *Journal of Sound and Vibration* 139 (1990) 241–252.
[31] K.M. Liew, C.M. Wang, Y. Xiang, S. Kitipornchai, *Vibration of Mindlin Plates*, Elsevier, Amsterdam, 1998.
[32] K.M. Liew, X. Zhao, T.Y. Ng, The element-free kp-Ritz method for vibration of laminated rotating cylindrical panels, *International Journal of Structural Stability and Dynamics* 2 (2002) 523–558.
[33] W.K. Liu, S. Jun, Y.F. Zhang, Reproducing kernel particle methods, *International Journal for Numerical Methods in Fluids* (1995) 1081–1106.
[34] J.N. Reddy, *An Introduction to the Finite Element Method*, McGraw-Hill, New York, 1993.